Supporting Information:

Structural Depended Electrode Property of Hollow Carbon Micro-Fibers Derived from platanus fruit and willow catkin for high performance supercapacitors

Hua Tan,[a] Xiaoning Wang,[a] Dedong Jia,[b] Pin Hao,[c] Yuanhua Sang,[a] Hong Liu[a]*

[a] State Key Laboratory of Crystal Material, Shandong University, Jinan 250100, PR China.

*E-mail: hongliu@sdu.edu.cn

[b] Beijing Institute of Nanosystems, Chinese Academy of Sciences, Beijing 100083, China.

[c] College of Chemistry, Chemical Engineering and Materials Science, Shandong Normal University, Jinan 250014, China.

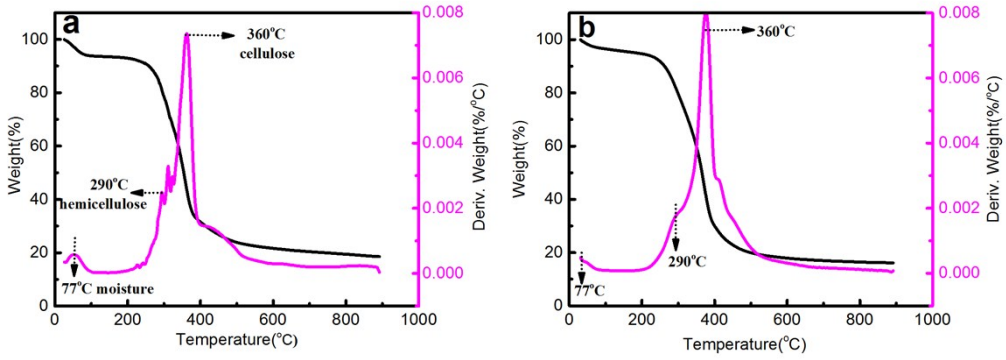

Fig. S1 TG/DTA curves of the PFs (a) and WFs (b) measured at a heating rate of 10°C/min in nitrogen atmosphere.

It is reported that the pyrolysis of the plant fibers is usually attributed to the pyrolysis of the cellulose, hemicellulose and lignin.[1, 2] Differential thermogravimetric (DTG) results of Platanus seed hollow fibers and willow catkin hollow fibers are shown in Fig. S1 a and b. In Fig. S1 a, it can be observed that the pyrolysis of the Platanus seed hollow fibers mainly occurred at the range of 200 °C to 600 °C. The peak at 77°C in the DTA curve is attributed to the removal of the physically adsorbed water and the dehydration of the Platanus seed hollow fibers.[3] The sharp decomposition peak at 360 °C with a shoulder at 290 °C is attributed to the thermal decomposition of the cellulose and hemicellulose, respectively. It is obvious that TG curve tends to flatten owing to the pyrolysis of the lignin at higher temperature.[4, 5] However, the lignin usually decomposes over a wide range without distinguishable peak. In Fig. S1 b, the TG/DTA curves of willow catkin hollow fibers has the similar tendency with the Platanus seed hollow fibers. At the low temperatures (77°C), the decomposition of the willow catkin hollow fibers is attributed to the physically adsorbed water and the dehydration of the willow catkin hollow fibers. The decompositions of the hemicellulose and cellulose are also concentrated at 360 °C and 290 °C. For the decomposition range of the lignin for willow catkin hollow fibers, the flatten of the TG curve occurred at 400 °C, which is smaller than that of the Platanus seed fibers (550 °C). It demonstrated that the Platanus seed hollow fibers have more stable structure than the willow catkin fibers, which is mainly due to the contents of the lignin and other elements. Therefore, in the carbonization section we mixed the temperatures at 900 °C and 800 °C for the Paltanus seed and willow catkin hollow fibers, respectively.

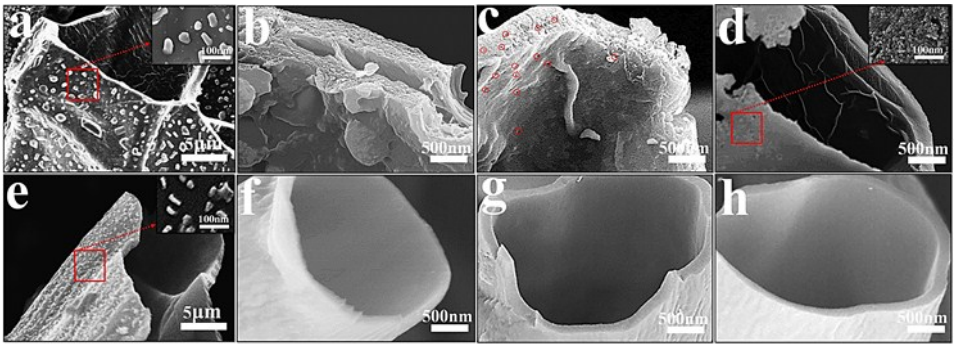

Fig. S2 SEM images of the carbonized Platanus fibers (a) and carbonized Platanus fibers activated by KOH at 800°C (PFs 800) (b), 900°C (PFs 900) (c), and 1000°C (PFs 1000) (d); and SEM images of carbonized willow catkin fibers (WFs) (e) and carbonized willow catkin fibers activated by KOH at 700°C (WFs 700) (f), 800°C (WFs 800) (g), and 900°C (WFs 900) (h).

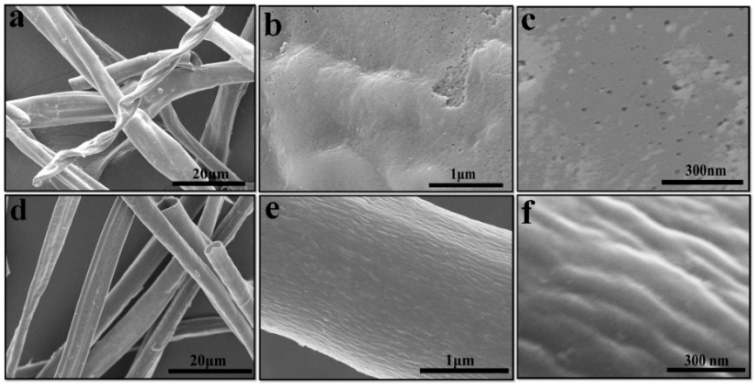

Fig. S3 SEM images of the carbonized PFs (a-c) and WFs (d-f) after being washed with deionized water.

As shown in Fig. S3 a-c, there are no solid particles on the surface of the PFs after being washed with deionized water. There were obviously amounts of meso/macropores on the surface of the carbonized PFs. In Fig. S3 d-f, no meso/macropores were found on the WFs hollow fibers after being treated with water and the hollow fibers have the rough surface distributed with amounts of channles. This result confirmed that the PFs have a relative violent self-activation functions just in the carbonization process.

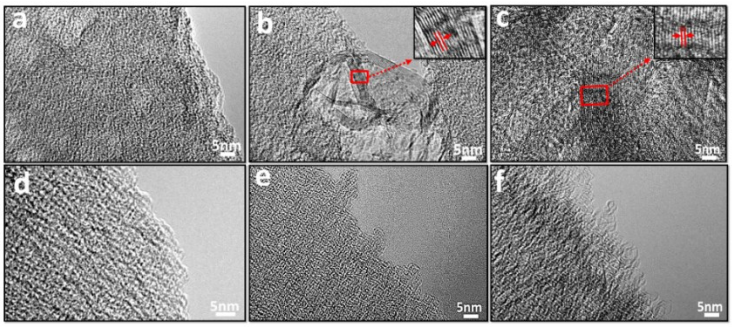

Fig. S4 High-Resolution TEM images of the PFs 800 (a), PFs 900 (b), PFs 1000(c) and WFs 700 (d), WFs 800 (e) and WFs 900(f).

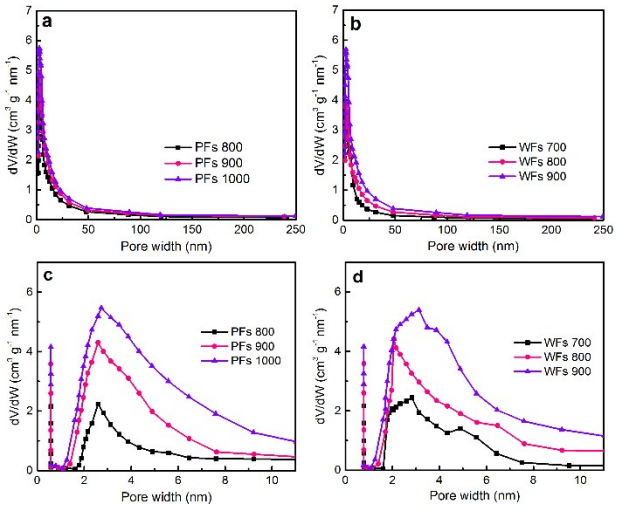

Fig. S5 Pore size distribution of the PFs (a) and WFs (b) activated at different temperatures (calculated by using BJH model), (c) detailed view of (a), (d) detailed view of (b).

Table S1 Physical properties obtained from the N_2 adsorption/desorption test

	PFs 800	PFs 900	PFs 1000	WFs 700	WFs 800	WFs 900
BET Surface area (m^2/g)	1167.7615	2014.8663	1717.5665	1065.4037	1697.3747	1492.4941
Average pore diameter (nm)	2.4318	1.9152	2.7234	2.7233	2.0158	3.0293
Total pore volume (cm^3/g)	0.5635	1.0973	1.1560	0.5139	0.9558	1.0133

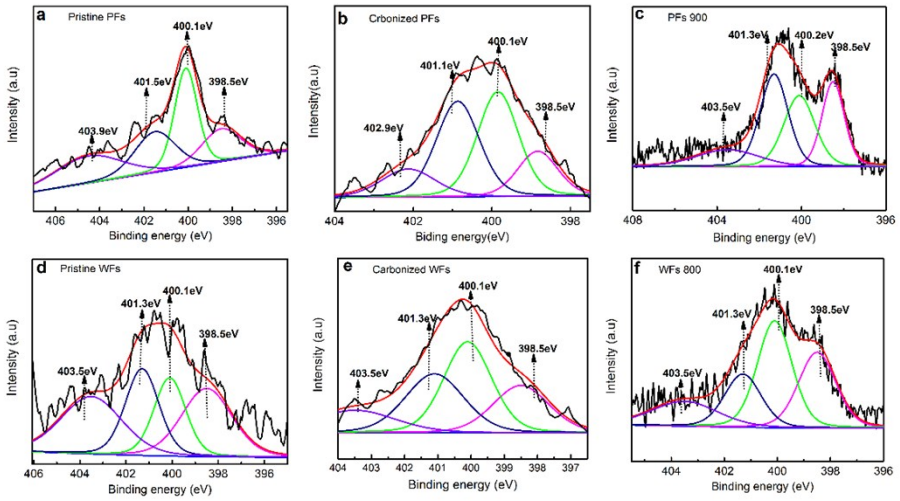

Fig. S6 High resolution N1s spectra and fitting peaks of pristine PFs (a), carbonized PFs (b), PFs 900 (c) and pristine WFs (d), carbonized WFs (e) and WFs 800 (f).

	Elemental analysis (wt%)				XPS analysis (atom%)				
Sample	C	H	N	S	C	N	O	S	Inorganic elements
Pristine PFs	57.98	6.071	1.201	0.167	58.64	1.082	12.65	0.154	0.752
Carbonized PFs	82.92	5.312	1.171	0.151	82.78	0.983	10.05	0.142	0.569
PFs 900	89.99	0.251	1.082	0.144	90.63	1.232	6.35	0.135	0.035
Pristine WFs	52.56	7.522	1.053	0.143	53.05	0.955	13.64	0.138	0.331
Carbonized WFs	80.65	6.213	0.985	0.126	81.23	0.884	11.23	0.127	0.113
WFs 800	84.45	0.362	0.954	0.118	85.13	1.132	7.63	0.109	0.021

Table S2 Elemental and XPS analysis of the PFs and WFs samples

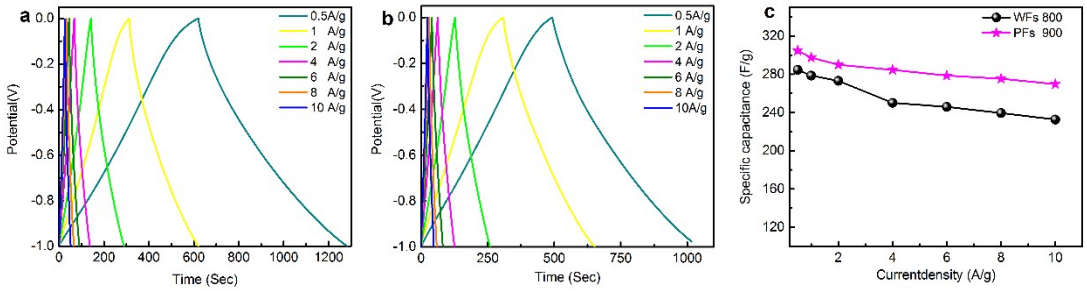

Fig. S7 GCD curves of PFs 900(a) and WFs 800(b) over a range of current densities from 0.5 to 10 A/ g; (c) specific capacitance as a function of the discharge current density for PFs 900 and WFs 800 in the three-electrode system

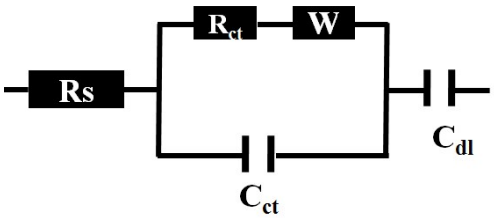

Fig. S8 Equivalent circuit model of Nyquist diagram for AC impedance measurement of the electrode.

As shown in **Fig. S8**, the equivalent circuit model is introduced to clarify the performance of the electrodes, where Rs represents the equivalent series resistance including the contact resistance between electrode leads, solution resistance and electrode resistance. Rct represents the charge transfer resistance, W is the Warburg impedance related to the ion diffusion in the electrolyte. Cct is the charge transfer capacitance and Cdl is the electrochemical double-layer capacitance in low frequency region.

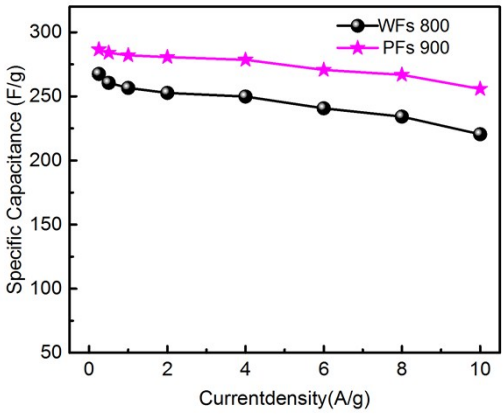

Fig. S9 Specific capacitance of PFs 900 and WFs 800 as a function of current density in the two-electrode system

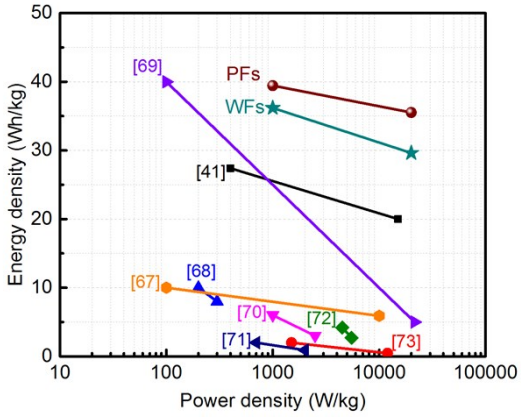

Fig. S10 Performance comparison of the WFs 800, PFs 900 in our work versus previously reported carbon symmetric supercapacitors in aqueous electrolyte.

References

1. S. Gaur and T. B. Reed, 1998.
2. K. Mansaray and A. Ghaly, *Bioresource technology*, 1998, **65**, 13-20.
3. J. Orfao, F. Antunes and J. L. Figueiredo, *Fuel*, 1999, **78**, 349-358.
4. A. J. Tsamba, W. Yang and W. Blasiak, *Fuel Processing Technology*, 2006, **87**, 523-530.
5. D. Vamvuka, E. Kakaras, E. Kastanaki and P. Grammelis, *Fuel*, 2003, **82**, 1949-1960.